Quantum-mechanical theory of field electron emission under axially symmetric forces

1998 J. Phys.: Condens. Matter 10 869

(http://iopscience.iop.org/0953-8984/10/4/015)

J. Phys.: Condens. Matter **10** (1998) 869–881. Printed in the UK PII: S0953-8984(98)84977-1

Quantum-mechanical theory of field electron emission under axially symmetric forces

A Mayer and J-P Vigneron

Laboratoire de Physique du Solide, Facultés Universitaires Notre-Dame de la Paix, rue de Bruxelles 61, B-5000 Namur, Belgium

Received 10 June 1997, in final form 17 October 1997

Abstract. Field emission from a metal nanotip is studied, because of its relevance to the modelling of the Fresnel projection microscope. This study includes the development of a new numerical approach to the axially symmetric Schrödinger equations.

1. Introduction

Tunnelling electrons encountering a potential barrier with axial symmetry have special properties, closely related to the nodal distribution of the eigenfunctions. These properties can often be exploited to facilitate the numerical solution of the one-body Schrödinger equation used to assess the electron current distribution for the discrete or continuous parts of its energy spectrum. Discrete states will not be discussed here, as this subject is amply discussed in most quantum chemistry textbooks. Rather, we will emphasize the incidence of the angular invariance on the continuous part of the spectrum, and use the conclusions to examine a microscopic model for the nanotip field emission.

The study is organized as follows. First, the consequences of the axial symmetry on the wavefunction are discussed and the set of coupled Schrödinger equations resulting from the symmetry specifications are derived. Next, the field-emission problem is formulated using a transfer-matrix approach. The modelling of field emission is discussed in section 3. SI units are used everywhere in this paper.

2. The axial symmetry

The axial symmetry is relevant to peculiar scattering problems, i.e. situations where the relevant parts of the system are invariant under any finite rotation. In this situation, the scattering problem is best formulated in cylindrical coordinates, choosing the symmetry axis as axial direction z. The polar coordinates in the plane normal to the symmetry axis are denoted ϕ (azimuthal angle) and ρ (radial distance to the axis). A first step to a numerical treatment of this problem consists of a discrete expansion of the wavefunction. In this context, it is natural to consider the complete set of eigenfunctions generated by the Schrödinger equation

$$-\frac{\hbar^2}{2m}\nabla^2\psi(\boldsymbol{r}) + V_0(z)\psi(\boldsymbol{r}) = E\psi(\boldsymbol{r}). \tag{1}$$

The potential $V_0(z)$ is considered independent of ϕ and ρ. The eigenfunctions are easily determined, and their set remains enumerable, as one specifies that the scattering electron remains localized inside a cylinder of radius R (preferably large compared with all electron wavelengths of interest) [1]. In this case, the basis functions are easily determined to factorize into

$$\psi_{m,j}(\boldsymbol{r}) = \Phi_{m,j}(z) J_m(k_{m,j}\rho)\left(2\pi \int_0^R \rho[J_m(k_{m,j}\rho)]^2 \, \mathrm{d}\rho\right)^{-1/2} \mathrm{e}^{\mathrm{i}m\phi}. \tag{2}$$

Here, the azimuthal quantum number m takes all negative and positive integer values, and j is another integer, which ranges from 0 to $+\infty$. These quantum numbers are used to enumerate the values of $k_{m,j}$ such that $J_m(k_{m,j}R) = 0$. This complete and orthogonal set of eigenfunctions provides a convenient basis to expand the sought standing wavefunctions in the axially symmetric three-dimensional scattering problem.

The full three-dimensional potential $V(\rho, z)$ is now assumed to have a radial dependence contained in an additional term $V_p(\rho, z)$, i.e. $V(\rho, z) = V_0(z) + V_p(\rho, z)$. With this assumption, the electron Schrödinger equation takes the form

$$-\frac{\hbar^2}{2m}\nabla^2\Psi(\boldsymbol{r}) + [V_0(z) + V_p(\rho, z)]\Psi(\boldsymbol{r}) = E\Psi(\boldsymbol{r}). \tag{3}$$

For this fully generalized equation, the eigenstates can be sought in the form of an expansion

$$\Psi(\boldsymbol{r}) = \sum_m \sum_j \Phi_{m,j}(z) J_m(k_{m,j}\rho)\left(2\pi \int_0^R \rho[J_m(k_{m,j}\rho)]^2 \, \mathrm{d}\rho\right)^{-1/2} \mathrm{e}^{\mathrm{i}m\phi} \tag{4}$$

where the coefficients satisfy the exact one-dimensional set of coupled equations

$$\frac{\mathrm{d}^2\Phi_{m,j}(z)}{\mathrm{d}z^2} + \left[\frac{2m}{\hbar^2}E - k_{m,j}^2 - \frac{2m}{\hbar^2}V_0(z)\right]\Phi_{m,j}(z) = \sum_{j'} M_{m,j}^{j'}(z)\Phi_{m,j'}(z). \tag{5}$$

The coupling coefficients are then obtained from

$$M_{m,j}^{j'}(z) = \frac{2m}{\hbar^2}\left(\int_0^R \mathrm{d}\rho\, \rho V_p(\rho, z) J_m(k_{m,j}\rho) J_m(k_{m,j'}\rho)\right)\left(\int_0^R \mathrm{d}\rho\, \rho[J_m(k_{m,j}\rho)]^2\right)^{-1/2} \times\left(\int_0^R \mathrm{d}\rho\, \rho[J_m(k_{m,j'}\rho)]^2\right)^{-1/2}. \tag{6}$$

Writing $V_0(z) + V_p(\rho, z)$ instead of $V(\rho, z)$ is useful, since the coupling coefficients corresponding to the ρ-independent part $V_0(\rho, z)$ of the potential analytically appear as $M_{m,j}^{j'}(z) = (2m/\hbar^2)V_0(z)\delta_{j,j'}$. Better precision in solving equation (5) is achieved if the main part of $V(\rho, z)$ appears in $V_0(z)$. The computation of the coupling coefficients $M_{m,j}^{j'}(z)$ is further simplified if $V_p(\rho, z)$ disappears for ρ greater than some ρ_{max} satisfying $\rho_{max} < R$.

Equation (5) is presented so that propagating terms are written on the left-hand side and coupling terms are moved to the right-hand side. It is apparent that the different terms in the wavefunction expansion in expression (4) do not mix with each other if the perturbing potential $V_p(\rho, z)$, dependent on ρ, vanishes. It is also straightforward that coupling occurs only between components with the same m subscripts. It is therefore possible to consider the diffusion problem for each m value separately.

The presence of Bessel functions in the expression of the $M_{m,j}^{j'}$ makes their computation very difficult. These should be evaluated for each value of z and used in equation (5). The numerical difficulties can be drastically reduced if the potential $V(\rho, z)$ (or its decomposition into $V_0(z) + V_p(\rho, z)$) is assumed to be constant over small steps in ρ and z. Analytical expressions (i.e. Lommel's formula [2]) can be used to compute $M_{m,j}^{j'}(z)$. These terms being constant over small steps in the z direction, special methods can be used to handle equation (5), i.e. discoupling this set of equations via an eigensystem method. This is discussed with further details in appendix A.

3. Field emission

Field emission [3–8] is basic to, among other uses, electron microscopy. The electron emission from metal surfaces was first explained by Fowler and Nordheim [3] in terms of quantum-mechanical events: the potential barrier which, under zero bias, prevents the electrons from escaping the metal is lowered by the applied electric field and the electron emission results from tunnelling across this lowered barrier.

The previously derived equations can be used in this specific problem, substituting existing theories without being confined to specific geometries [9–11] (planar, hyperboloids, . . .). Our method, based on the numerical solution of equations (5) and (6), does not imply the usual modelling restrictions.

The subject of this section will be the field emission obtained through the use of nanotips [12–16]. These small tips, whose height is of the order of 2 nm, usually stand on the top of a tungsten larger tip. These tips are those used to operate the Fresnel projection microscope (FPM) [17, 18]. The field is obtained from an electric bias established between the tip and a conducting grid a few tens of nanometres apart. This field is responsible for the appearance of an electronic micro-beam. In the FPM, a molecule can be placed in this beam, producing a 'shadow' [19] observable on a macroscopically distant screen.

Field emission from small tips also finds applications in flat panel displays [27–29]. They consist of large arrays of microscopic tips facing a grid. The bias between the grid and the support of the tips is responsible for a field-emission process. A relevant theory would allow the computation of the current obtained by such displays for a given bias.

The high coherence [26] of electrons field emitted by the nanotips gives physical consistence to the equations of section 2. However, since the electrons are confined inside a microscopic cylinder, the results of these calculations will have physical meaning only at microscopic distance from the emitting tip, where the wavefunction cancellation condition at $\rho = R$ is acceptable. Let us study the field-emission process from such nanotips.

For simplicity, the tip will be represented by a cone standing on a semi-infinite metal delimited by a plane. The symmetry z-axis will be placed at the centre of the cone with $z = 0$ coinciding with the plane surface of the infinite metal substrate, assuming the existence of an electric bias V between this and the grid at $z = D$. Let us suppose the potential to be constant beyond this plane (D being large enough, with no bias between the grid and a hypothetical distant screen). The tip metal is described here using a simple Sommerfeld picture, characterized by empirical values of W (work function) and E_F (Fermi energy). The dielectric constant ε_r takes infinite values inside the metal.

This situation of complete symmetry around the z-axis is relevant to equations (5) and (6). The field-emission phenomenon will result in the production of an electronic beam mainly confined to the z-axis region. The hypothesis of the wavefunction cancellation beyond $\rho = R$ is therefore acceptable, if R is chosen large enough. It appears in the simulations that the main contribution to the wavefunction comes from coefficients pertaining to $m = 0$. This means that only a limited number of m values need be considered.

The first step here is to perform a computation of the potential distribution. It is considered constant beyond $z = D$ where its value will conventionally be set to zero. For negative z values and inside the metallic tip, the potential energy is $(V - W - E_F)$. The electrostatic potential in the intermediate region $0 < z < D$ is obtained by application of an over-relaxation method [20] (presented in appendix B), taking into account the axial invariance and the non-uniformity of the dielectric constant ε_r. The bias V between the two planes $z = 0$ and $z = D$ gives the boundary conditions. The image potential is also numerically computed (cf [20]) and incorporated into the former calculated electrostatic potential.

The next step is to obtain the transfer matrix [21, 22] of the system. It is known from expression (4) that the wavefunction can be expanded into a series which can be seen as a superposition with coefficients $\Phi_{m,j}(z)$ of the basis functions:

$$J_m(k_{m,j}\rho)\left(2\pi\int_0^R \rho[J_m(k_{m,j}\rho)]^2\,\mathrm{d}\rho\right)^{-1/2} \mathrm{e}^{\mathrm{i}m\phi}. \tag{7}$$

In the metal ($z < 0$) and beyond the grid ($z > D$), the coefficients $\Phi_{m,j}(z)$ appear, following equation (5), to be simple plane waves describing electron propagation towards negative or positive z values if they are not real exponential functions. This is due to the electron confinement in a cylinder, which is invariant along z, and is another indication that the confinement hypothesis is relevant only for distances of the order of R. In the FPM, the wavefunction would become, at greater distances, a superposition of spherical waves, due to the central asymptotic potential at macroscopic scales.

The range of j subscript considered is limited here by the condition $(\hbar^2/2m)k_{m,j}^2 \leqslant E$, so that only travelling plane waves are present in $\Phi_{m,j}(z)$ in the region $z > D$.

In order to obtain the transfer matrices, each outgoing basis function in the region $z > D$ has to be considered individually. In all cases, there is no basis function in the region $z > D$ coming back from $z = +\infty$. Knowing the wavefunction at $z = D$, using equations (5) and (6), the wavefunction can be constructed at $z = 0$ and decomposed into elementary basis functions coming from or going to $z = -\infty$. The ρ-independent part $V_0(z)$ of the potential distribution $V(\rho, z)$ computed in the first step takes the value $V_0(z) = V(R, z)$.

It has already been noted that basis functions characterized by different m subscripts propagate without interaction. It is consequently allowable to treat all m values individually. The basis functions are characterized by their radial wavevector $k_{m,j}$. The amplitude of the plane wave associated with the coefficients $\Phi_{m,j}(z)$ of the wavefunction representation are assembled as vectors, where the coefficients corresponding to positive $k_{m,j}$ values are taken first and the ones corresponding to negative $k_{m,j}$ values are taken last. The coefficients are each time classified according the j subscript. Let $A_{m,j}$ $(B_{m,j})$ be the amplitude of the plane wave corresponding to $k_{m,j}$ with positive (negative) z oriented wavevector. Due to linearity, the coefficients of a wavefunction expansion at $z = 0$ can be linearly related to the corresponding coefficients at $z = D$:

$$\begin{pmatrix} (A_{m,j})_j \\ (B_{m,j})_j \end{pmatrix}_{z=0} = \begin{pmatrix} (M) & (N) \\ (O) & (P) \end{pmatrix} \begin{pmatrix} (A_{m,j})_j \\ (B_{m,j})_j \end{pmatrix}_{z=D}. \tag{8}$$

Taking incident wavefunctions with unit amplitude and reminding the absence of plane waves coming back from $z = +\infty$, the above relations reduce to:

$$\begin{pmatrix} (I) \\ (t^{-+}) \end{pmatrix} = \begin{pmatrix} (M) & (N) \\ (O) & (P) \end{pmatrix} \begin{pmatrix} (t^{++}) \\ (O) \end{pmatrix} \tag{9}$$

which are solved to give

$$\begin{aligned} (t^{++}) &= (M)^{-1} \\ (t^{-+}) &= (O)(M)^{-1}. \end{aligned} \tag{10}$$

The matrix (t^{++}) gives the amplitudes of the transmitted basis functions for each incident basis function with unit amplitude at $z = 0$. The matrix (t^{-+}) gives the amplitudes for the corresponding reflected basis functions. The matrices (M) and (O) are simply obtained after propagation of each basis function from $z = D$ to $z = 0$.

This method, which assumes an efficient treatment of equations (5) and (6), is very stable because the numerical integration (towards negative z values) is carried out in the direction opposite to the physical wave propagation (towards positive z values). In fact, a one-dimensional potential barrier in tunnelling problems gives rise to a pair of evanescent waves propagating against each other. Both waves are evanescent in their natural propagation direction but increase exponentially in the opposite direction. Numerically, for a chosen integration direction, the growing solution will dominate the diminishing wave, forcing the integration to be done so that the dominant solution is the physical one.

For a wide potential barrier, it is not always possible to compute in a single step the transfer matrices corresponding to the total distance D. In these cases, the interval D can be divided into smaller slabs. Four transfer matrices computed for each slab, namely (t^{-+}) and (t^{++}), as considered previously and (t^{--}) and (t^{+-}) which describe the behaviour of an incident wave travelling from $z = +\infty$. Pendry [23] developed a very efficient procedure to assemble constitutive slabs for this system. Another method to stabilize the computation is to exclude for each slab the waves whose normal energy $E - (\hbar^2/2m)k^2_{m,j}$ is too small. These waves are considered to be completely reflected, by forcing the value of the transfer matrices expressing reflection ((t^{-+}) and (t^{+-})).

Once the transfer matrix of the total system is known (the region $0 < z < D$ and the metal), it is easy to compute the particle probability density in the region $z > D$. Each incident basis function in $z = 0$ has to be considered individually, using the transfer matrix (t^{++}) to obtain the corresponding wavefunction in the region $z > D$, computing the corresponding intensity $|\Psi_{m,j}(\rho, \phi, z)|^2$. A weighted sum of particle densities is then performed (contrasting with a weighted sum of amplitudes). The reason of this loss of coherence is the absence of correlation between the incoming electrons. The observed intensity is contributed by all the incoming electrons, each of them participating in an independent experiment.

The weight to each incoming basis function is taken to be its contribution to the total density of states at the Fermi level E_F for electrons captured in a cylinder of radius R:

$$D(E_F) = \frac{8m}{(Rh)^2} \sum_m \sum_j \frac{1}{\sqrt{2mE_F/\hbar - k^2_{m,j}}} \tag{11}$$

where all quantities have already been defined. This expression is derived in appendix C.

The current density can be obtained in a similar way. This is done by using the expression for the current density $\boldsymbol{J}$ associated with a wavefunction Ψ:

$$\boldsymbol{J}(\boldsymbol{r}) = \frac{1}{m}\mathrm{Re}\left[\Psi(\boldsymbol{r})^*\left(\frac{\hbar}{\mathrm{i}}\boldsymbol{\nabla}\Psi(\boldsymbol{r})\right)\right]. \tag{12}$$

In cylindrical coordinates, there is no dependence on the azimuthal angle ϕ because $m = 0$ does not contribute to J_ϕ and because contributions due to non-zero opposite m values cancel out.

The procedure is clearly similar to that adopted for the computation of the intensity. A weighted sum of the current density corresponding to each incident basis function in the metal is performed. The weights are the same as those used for the particle density.

There are two important points to notice. First, the 'current density' as obtained is a quantum-mechanical concept associated with the electron wavefunctions at Fermi level.

By contrast, the electric current density $\boldsymbol{j}(\boldsymbol{r})$ of physical significance contains the electron charge e and gathers contributions from electrons with all possible energy E. The relevant relation is

$$\frac{\partial j(\boldsymbol{r})}{\partial E} = e\boldsymbol{J}(\boldsymbol{r}, E) \tag{13}$$

where $\boldsymbol{J}(\boldsymbol{r}, E)$ is the quantum-mechanical current density obtained by considering electrons with energy E. In order to obtain $\boldsymbol{j}(\boldsymbol{r})$, $\boldsymbol{J}(\boldsymbol{r}, E)$ has to be computed at Fermi level E_F and other energy levels below E_F and an integration has to be performed.

The second point is the importance of a correct wavefunction normalization in order to correctly evaluate $\boldsymbol{j}(\boldsymbol{r})$, on an absolute scale. The idea is to multiply each wavefunction obtained by this method by the same normalization coefficient A, requiring us to obtain the correct electron density inside the metal. This choice of the normalization allows the probability to find an electron in a given section of the cylinder to be the same for each basis function (7).

With a Sommerfeld free electron metal, the Fermi energy E_F is related to the electron density ρ_{elec} through the relation

$$E_F = \frac{\hbar^2}{2m}[3\pi^2\rho_{elec}]^{2/3}.$$

The electron density is assumed to be constant in the cylinder of radius R.

The electron density can also be obtained by an integration (sum) of $|\Psi|^2$ over all occupied states. In representation (4), this becomes

$$\rho_{elec}(\boldsymbol{r}) = \int_0^{E_F} \mathrm{d}E \sum_m \sum_j \frac{8m}{(Rh)^2} \frac{1}{\sqrt{2mE/\hbar^2 - k_{m,j}^2}} |A|^2 J_m(k_{m,j}\rho)^2 \times \left(2\pi \int_0^R \rho [J_m(k_{m,j}\rho)]^2 \,\mathrm{d}\rho\right)^{-1}. \tag{14}$$

This expression assumes zero temperature (no occupied states above the Fermi level). Evaluating this expression on the z axis ($\rho = 0$), it becomes

$$\rho_{elec} = |A|^2 \frac{8m}{(Rh)^2} \int_0^{E_F} \mathrm{d}E \sum_j \frac{1}{\sqrt{2mE/\hbar^2 - k_{0,j}^2}} \left(2\pi \int_0^R \rho [J_0(k_{0,j}\rho)]^2 \,\mathrm{d}\rho\right)^{-1}. \tag{15}$$

The integration over E is easily performed. Actually, considering all possible j and E values (up to E_F), it is possible to swap the sum over j and the integration over E, so that the integration is almost immediate. Knowing the electron density ρ_{elec}, the normalization coefficient A is derived from equation (15).

4. Results

The dimensions of the nanotip are 1 nm for the basis radius and 2 nm for the height. In order to allow a comparison with former computations [4], relevant to a tungsten planar emitter, the same parameters were taken, i.e. a work function W of 4.5 eV and a Fermi energy E_F of 5.8 eV. The grid is set at the distance $D = 15$ nm with an electrical potential of 30 V, with respect to the metal tip. The wavefunction cancellation radius R is taken equal to 15 nm. The first figure shows the considered geometry.

Figure 2 shows the particle probability density (i.e. $|\Psi(\boldsymbol{r})|^2$) corresponding to incident waves characterized by m subscript ranging from -2 to $+2$, as a function of ρ for $z = D$. The maximum value is normalized to unity and the image potential is not accounted for.

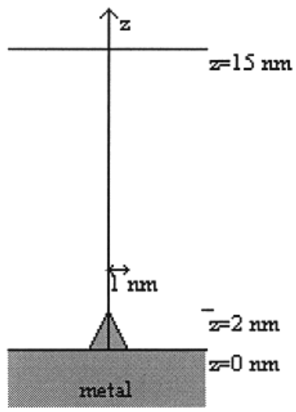

Figure 1. Schematic representation of the metal (limited by the plane $z = 0$ nm), the tip and the grid (represented by the plane $z = 15$ nm).

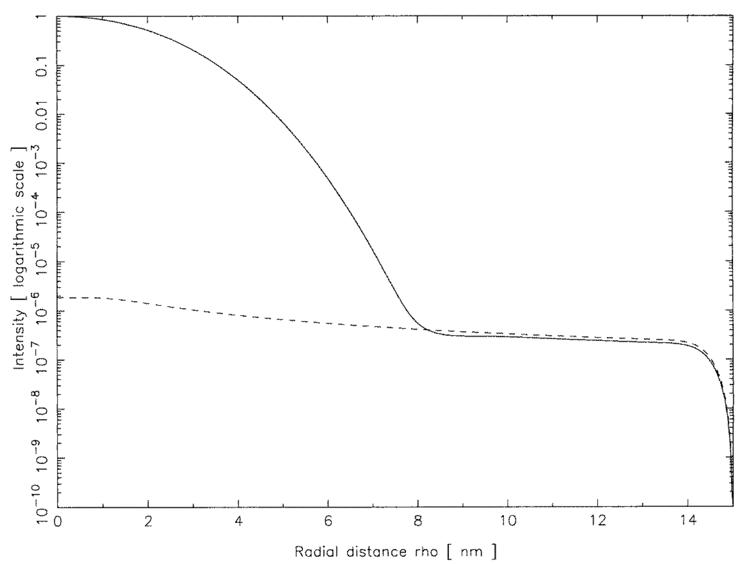

Figure 2. Normalized particle probability density at $z = 15$ nm, considering only states described by $m = 0$, ± 1 or ± 2, without image potential. The dotted curve is an analytic result with no tip.

The dotted curve corresponds to the particle probability density one would analytically obtain if the potential distribution in the region $0 < z < D$ were linear (i.e. no tip and no image contribution). Excellent agreement is obtained in the right part of the figure, where the tip induced potential perturbation becomes negligible. This region corresponds to electrons tunnelling across the triangular potential barrier. The intensity enhancement at $\rho = 0$ due to the tip is around 500 000.

The effects of the artificial wavefunction vanishing condition $\Psi(\rho, \phi, z) = 0$ for $\rho \geqslant R$ are restricted to the vicinity of $\rho = R$. No change is observed in the wide central part of the scattering domain.

The contribution of the tip (appearing at the left side of the picture) appears to be very important for $m = 0$ and almost negligible for $|m| = 2$. This is due to the fact that the basis functions corresponding to high $|m|$ values are very small in the region near $\rho = 0$, where the tip potential perturbation is confined. This effect has already been observed in scanning tunnelling microscopy simulations using the Green function formalism [24] and justifies the restriction in the considered m values for this field emission situation. The effect of the neglected m values is to bring the right side of the figure closer to the tipless $\rho = 0$ current.

Figure 3 shows the particle probability density obtained when the image potential is included, for incident basis functions characterized by m subscripts ranging from -2 to $+2$ and z values of D.

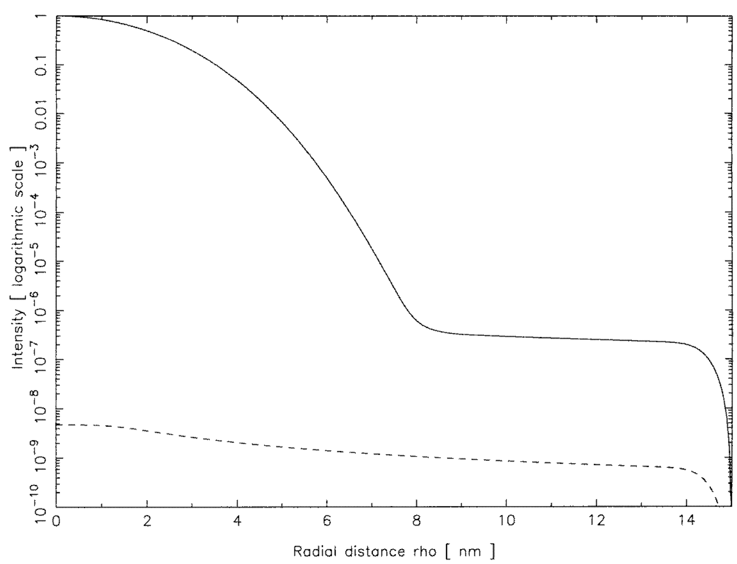

Figure 3. Normalized particle probability density at $z = 15$ nm, considering only states described by $m = 0$, ± 1 or ± 2, with image potential. The dotted curve is an analytic result with no tip.

The image potential enhances the particle presence probabilities by a factor of 300 (compared to the values obtained without tip and image potential). This effect is related to the decrease of the potential barrier in front of the metal. The emerging electrons describe a beam with half-opening angle of 4.5° (by considering the current density orientation). This corresponds typically to the experimental values obtained at macroscopic distances with similar tips but somewhat larger values for the bias and distance D. This half-opening angle, evaluated at the grid, was found to become smaller with increasing metal–grid distances or diminishing bias. Changing the tip dimensions also modifies it. Increasing the tip radius or reducing the tip height results in a lower half-opening angle. The self-collimation effect observed in the FPM [30, 31] is due to the long-range influence of the base tip on the potential. This is not considered here.

Figure 4 shows the z component of the current density (obtained by energy integration of 1 eV below the Fermi level). The current density value for large ρ is in good agreement with the calculations of Good *et al* [4] for field emission by a planar emitter.

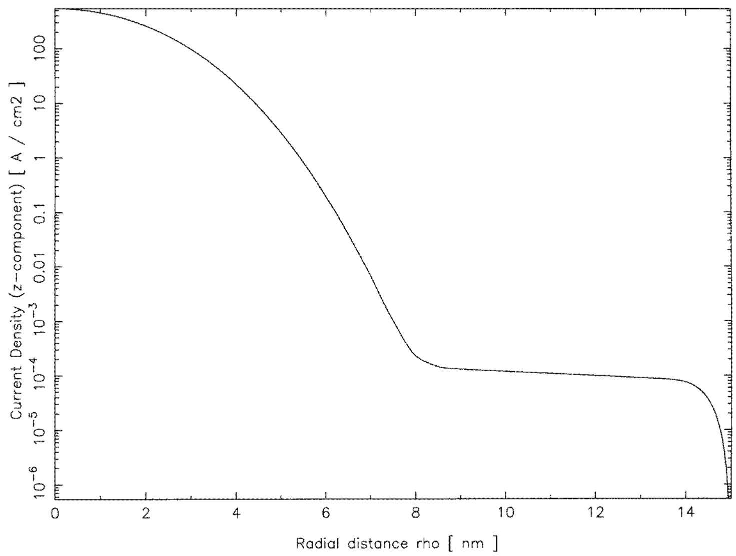

Figure 4. Current density at $z = 15$ nm, considering only states described by $m = 0, \pm 1$ or ± 2, with image potential.

5. Conclusion

A method to compute elastic scattering in the presence of rotational invariance was presented, assuming a reasonable boundary condition adequate for tunnelling problems. This method was applied to a field-emission problem. Since the only information needed is the axially symmetric potential energy distribution, it can be applied to many kinds of field-emission situation with rotational invariance.

This method has some advantages over the Green formalism [24, 25] in situations where the potential perturbation cannot be considered localized in space. In fact, the Green formalism requires the creation of a matrix whose size corresponds to the square of the number of perturbed potential elements. Here, this number would appear to be proportional to $E^2R^2D^2$. Such a matrix is not needed here. On the other hand, the computation of the coupling coefficients $M^{j'}_{m,j}(z)$ requires arrays whose size depends on the number of basis functions and on the number of discretization steps in R. This number appears to be proportional to $E^{3/2}R^3$. The computations performed here are out of reach of the Green formalism with the present state of computers.

This method is limited to regions where the wavefunction cancellation condition is physically admissible. Further work is needed to obtain the current density at long (macroscopic) distances from the source.

Acknowledgments

AM was supported by the Belgian National Fund for Scientific Research (FNRS). J-PV acknowledges the national programme for Interuniversity Research Projects (PAI). The authors acknowledge the use of the Namur Scientific Computing Facility, a common project between the FNRS, IBM—Belgium and the FUNDP. We are grateful to L Philippe, Ph Lambin, M Devel and Ch Girard for useful discussions.

Appendix A. Eigensystem method for wavefunction propagation

Let us consider the propagation equation

$$\frac{\mathrm{d}^2\Phi_{m,j}(z)}{\mathrm{d}z^2} + \left[\frac{2m}{\hbar^2}E - k_{m,j}^2 - \frac{2m}{\hbar^2}V_0(z)\right]\Phi_{m,j}(z) = \sum_{j'} M_{m,j}^{j'}(z)\Phi_{m,j'}(z).$$

The subscripts m are not really needed, as coefficients $\Phi_{m,j}(z)$ with different m values are not coupled. It is important to notice that the coupling coefficients $M_{m,j}^{j'}(z)$ are real, symmetric in j and j'. These coefficients define, for each m and z value, a symmetric matrix. Their eigenvalues are real and their eigenvectors are orthonormal.

Let us assume the potential $V(\rho, z)$ varies discontinuously along z with constant values on small steps, i.e. $V(\rho, z)$ has no z dependence on the step Δz. The coupling coefficients $M_{m,j}^{j'}(z)$ are constant on this step and take the value $M_{m,j}^{j'}(\Delta z)$. Let us consider the vector $\bar{\Phi}_m(z)$, containing all $\Phi_{m,j}(z)$ coefficients.

The system of coupled equations can be rewritten as

$$\frac{\mathrm{d}^2}{\mathrm{d}z^2}\bar{\Phi}_m(z) + (E)\bar{\Phi}_m(z) = (M)\bar{\Phi}_m(z)$$

where (E) is a diagonal matrix containing the elements $(2m/\hbar^2)E - k_{m,j}^2 - (2m/\hbar^2)V_0(\Delta z)$ and (M) is a matrix containing the elements $M_{m,j}^{j'}(\Delta z)$.

$(E) - (M)$ being a real symmetric matrix, its eigenvalues are real and there exists an orthonormal basis of associated eigenvectors. Let (U) be the unitary matrix containing in columns the $(E) - (M)$ eigenvectors and (λ) the diagonal matrix containing the corresponding eigenvalues. $(E) - (M)$ can be replaced by $(U)(\lambda)(U)^*$.

Let us define $\bar{\Delta}_m(z) = U^*\bar{\Phi}_m(z)$. The propagation equation becomes

$$\frac{\mathrm{d}^2}{\mathrm{d}z^2}\bar{\Delta}_m(z) + (\lambda)\bar{\Delta}_m(z) = 0.$$

This system of uncoupled equations is easily solved and allows for an analytical propagation of $\bar{\Delta}_m(z)$ over Δz. $\bar{\Phi}_m(z)$ is retrieved by the relation $\bar{\Phi}_m(z) = U\bar{\Delta}_m(z)$.

Appendix B. Computation of electrostatic potential in cylindrical coordinates assuming a total rotational symmetry axis

Let us define a three-dimensional grid in cylindrical coordinates $(i\Delta\rho, j\Delta z, k\Delta\phi)$, where the steps along ρ, z and ϕ are constant. Due to the total axial symmetry around the z axis, the last coordinate will not need to be considered. As general notation, $f_{i,j}$ will be used for $f(i\Delta\rho, j\Delta z)$.

Assuming no charge density (included in the image potential), one obtains from the Maxwell equations

$$\boldsymbol{\nabla}\cdot[\varepsilon(\boldsymbol{r})\boldsymbol{\nabla}V(\boldsymbol{r})] = 0.$$

or

$$\boldsymbol{\nabla}\varepsilon(\boldsymbol{r})\cdot\boldsymbol{\nabla}V(\boldsymbol{r}) + \varepsilon(\boldsymbol{r})\Delta V(\boldsymbol{r}) = 0.$$

Cylindrical coordinate expression of the gradient and Laplacian is then used, assuming no ϕ dependence for all variables. The discrete expression for $\Delta V(\boldsymbol{r})$ in cylindrical coordinates is

$$\frac{1}{\Delta\rho^2}\left(1+\frac{1}{2\mathrm{i}}\right)V_{i+1,j}+\frac{1}{\Delta\rho^2}\left(1-\frac{1}{2\mathrm{i}}\right)V_{i-1,j}+\frac{1}{\Delta z^2}V_{i,j+1}+\frac{1}{\Delta z^2}V_{i,j-1} - \left(\frac{2}{\Delta\rho^2}+\frac{2}{\Delta z^2}\right)V_{i,j}.$$

The scalar product $\boldsymbol{\nabla}\varepsilon(\boldsymbol{r})\cdot\boldsymbol{\nabla}V(\boldsymbol{r})$ contains the derivative $\partial\varepsilon/\partial\rho$ approached by

$$\frac{\varepsilon_{i+1,j}-\varepsilon_{i-1,j}}{2\Delta\rho}$$

while $\partial V/\partial\rho$ is written

$$\frac{V_{i+1,j}-V_{i,j}}{\Delta\rho} \qquad \text{when associated with the term } \varepsilon_{i+1,j}$$

or

$$\frac{V_{i,j}-V_{i-1,j}}{\Delta\rho} \qquad \text{when associated with the term } \varepsilon_{i-1,j}.$$

Similar expressions are used for partial derivatives along z.

The final result reads

$$\begin{aligned} V_{i,j} = \{&\Delta z^2(\varepsilon_{i+1,j}+\varepsilon_{i,j}(2+1/\mathrm{i}))V_{i+1,j}+\Delta z^2(\varepsilon_{i-1,j}+\varepsilon_{i,j}(2-1/\mathrm{i}))V_{i-1,j} \\ &+\Delta\rho^2(\varepsilon_{i,j+1}+2\varepsilon_{i,j})V_{i,j+1}+\Delta\rho^2(\varepsilon_{i,j-1}+2\varepsilon_{i,j})V_{i,j-1}\} \\ &\times\{\Delta z^2(\varepsilon_{i+1,j}+\varepsilon_{i-1,j})+\Delta\rho^2(\varepsilon_{i,j+1}+\varepsilon_{i,j-1})+4(\Delta\rho^2+\Delta z^2)\varepsilon_{i,j}\}^{-1}. \end{aligned}$$

For points located on the Z axis ($i = 0$), symmetry considerations lead to the result

$$V_{0,j} = \frac{\Delta z^2 2(\varepsilon_{1,j}+2\varepsilon_{0,j})V_{1,j}+\Delta\rho^2(\varepsilon_{0,j+1}+2\varepsilon_{0,j})V_{0,j+1}+\Delta\rho^2(\varepsilon_{0,j-1}+2\varepsilon_{0,j})V_{0,j-1}}{\Delta z^2 2\varepsilon_{0,j}+\Delta\rho^2(\varepsilon_{0,j+1}+\varepsilon_{0,j-1})+4(\Delta\rho^2+\Delta z^2)\varepsilon_{0,j}}.$$

The boundary conditions being defined, the last two formulas are applied iteratively until convergence is reached.

The number of iterations can be reduced by iterating a combination of new and old potential values. A classic over-relaxation method (with potential changes weighted with ($\alpha = 1.9$) was used to carry out the iterative scheme.

Appendix C. Density of states in a cylinder of radius *R*

Let us consider a cylinder of radius R and length L. This cylinder is assumed to be occupied with electrons, whose kinetic energy ranges from 0 to E.

The different possible states along ρ are described by the eigenfunctions

$$J_m(k_{m,j}\rho)\left(2\pi\int_0^R \rho[J_m(k_{m,j}\rho)]^2\,\mathrm{d}\rho\right)^{-1}\mathrm{e}^{\mathrm{i}m\phi}$$

where the radially oriented wavevector $k_{m,j}$ satisfies the property $J_m(k_{m,j}R) = 0$ and is limited by $\sqrt{2mE/\hbar^2}$. All m values, compatible with the existence of a $k_{m,j}$ value have to be considered.

Considering the limit E to the kinetic energy, the axially oriented wavevector k_z associated with a value $k_{m,j}$ ranges from $-\sqrt{2mE/\hbar^2 - k_{m,j}^2}$ to $\sqrt{2mE/\hbar^2 - k_{m,j}^2}$.

Recalling the physically imposed distance $2\pi/L$ between two successive states along k_z and taking account of the two possible spin orientations, the total number of states in the cylinder is

$$2\frac{L}{2\pi}2\sum_m\sum_j\sqrt{\frac{2mE}{\hbar^2} - k_{m,j}^2}.$$

The number of electronic states per unit volume, for kinetic energy ranging from 0 to E, will be denoted $N(E)$ and is obtained by dividing this last number by the cylinder volume $\pi R^2 L$.

The density of states for kinetic energy E, denoted $D(E)$, is defined by the relation

$$\mathrm{d}N(E) = D(E)\,\mathrm{d}E.$$

Its expression is easily derived:

$$D(E) = \frac{2m}{(R\pi\hbar)^2}\sum_m\sum_j\frac{1}{\sqrt{2mE/\hbar^2 - k_{m,j}^2}}.$$

References

[1] Laloyaux T 1993 *Phys. Rev.* B **47** 7508–18
[2] Watson G N 1966 *Theory of Bessel Functions* 2nd edn (Cambridge: Cambridge University Press)
[3] Fowler R H and Nordheim L 1928 *Proc. R. Soc.* A **119** 173–81
[4] Good R H and Müller E W 1956 *Handbuch der Physik* vol 21, pp 176–231
[5] Burgess R E, Kroemer H and Houston J M 1953 *Phys. Rev.* **90** 515
[6] Young D R 1959 *Phys. Rev.* **113** 110–14
[7] Stratton R 1964 *Phys. Rev.* **135** A794–A805
[8] Swanson L W and Crouser L C 1967 *Phys. Rev.* **163** 622–41
[9] He J, Cutler P H, Miskovsky N M, Feuchtwang T E, Sullivan T E and Chung Moon 1991 *Surf. Sci.* **246** 348–64
[10] Cutler P H, He J, Miskovsky N M, Sullivan T E and Weiss B 1992 *J. Vac. Sci. Technol.* B **11** 387–91
[11] Jensen K L and Zaidman E G 1993 *J. Vac. Sci. Technol.* B **12** 776–80
[12] Bin V T, Purcell S T, Garcia N and Doglion I 1992 *Phys. Rev. Lett.* **69** 2527–30
[13] Purcell S T, Binh V T, Garcia N, Lin M E, Andres R P and Reifenberger R 1994 *Phys. Rev.* B **49** 17 259–63
[14] Garcia N, Binh V T and Purcell S T 1993 *Surf. Sci. Lett.* **293** 884–6
[15] Binh V T, Garcia N, Purcell S T and Semet V 1993 *Nanosources and Manipulation of Atoms Under High Fields and Temperatures: Applications* (Deventer: Kluwer)
[16] Binh V T and Garcia N 1994 *Surf. Sci.* **320** 69–75
[17] Binh V T, Semet V and Garcia N 1995 *Ultramicroscopy* **58** 307–17
[18] Fink H-W, Stocker W and Schmid H 1990 *Phys. Rev. Lett.* **65** 1204–6
[19] Melmed A J 1968 *Appl. Phys. Lett.* **12** 100–2
[20] Laloyaux T 1993 *Phys. Rev.* B **47** 7508–18
[21] Vigneron J-P, Derycke I, Laloyaux T, Lambin P and Lucas A A 1993 *Scanning Microsc. Suppl.* **7** 261–8
[22] Sheng W D and Xia J B 1996 *J. Phys.: Condens. Matter* **8** 3635–45
[23] Pendry J B 1994 *J. Mod. Opt.* **41** 209–29
[24] Lucas A A, Morawitz H, Henry G R, Vigneron J P, Lambin P, Cutler P H and Feuchtwang T E 1988 *Phys. Rev.* B **37** 10 708–20
[25] Martin O J F, Girard C and Dereux A 1995 *Phys. Rev. Lett.* **74** 526–9
[26] Garcia N and Rohrer H 1989 *J. Phys.: Condens. Matter* **1** 3737
[27] Brenac A, Baptist R, Chauvet G and Meyer R 1987 *Revue Phys. Appl.* **22** 1819–34
[28] Johnston R 1991 *Surf. Sci.* **246** 64–8

[29] Delong A 1993 *Eur. Microsc. Anal.* November 1993 **27** 9–11
[30] Binh V T, Garcia N and Purcell S T 1996 *Advances in Imaging and Electron Physics* vol 95 (New York: Academic) p 63
[31] Rose D J 1956 *J. Appl. Phys.* **27** 215